Journal of Applied Polymer Science

Cocontinuous Morphology in Vinylidene Fluoride Based Polymers/Poly(ethylene oxide) Blends

V. Daux, F. Prochazka, C. Carrot
Université de Lyon, F-42023, Saint-Etienne, France
Centre National de la Recherche Scientifique, Unité Mixte de Recherche 5223, Ingénierie des Matériaux Polymères, Saint-Etienne F-42023, France
Université de Saint-Etienne, Jean Monnet, Saint-Etienne F-42023, France
Correspondence to: F. Prochazka (E-mail: prochazk@univ-st-etienne.fr)

ABSTRACT: In this work, blends of three different vinylidene fluoride (VdF) based homopolymers and copolymers with poly(ethylene oxide) were investigated. We focused on the continuity domain and, more particularly, on the cocontinuous morphology of these systems. The melt-mixed blends were characterized by different techniques. The morphology was identified through a selective extraction technique and was confirmed by scanning electron microscopy. Dynamic oscillatory shear measurements were performed with a constant stress rheometer in the linear viscoelastic domain in the whole composition range. Because of the high viscosities and long relaxation times of the VdF-based polymers, the interfacial effects were hidden by the intrinsic behavior of the neat components. Nevertheless, the combination of the different techniques highlighted the similarity of the systems toward morphological development, whatever the VdF monomers. The experiments and theoretical analysis indicated that the rheological behavior dominated the interfacial effects in such systems with a large viscosity ratio and that it also dictated the boundaries of the continuity domain. The originality of this study came from the use of three different VdF-based polymers. © 2012 Wiley Periodicals, Inc. J. Appl. Polym. Sci. 000: 000–000, 2012

KEYWORDS: blends; morphology; rheology

Received 27 January 2012; accepted 8 June 2012; published online
DOI: 10.1002/app.38167

INTRODUCTION

The blending of polymers has become one of the most relevant methods for obtaining new high-performance materials in polymer science. These alloys are an alternative to conventional polymers in various fields. Indeed, this technique allows one to tailor the physical and chemical properties according to the requirements of the final application by reducing the cost induced by the synthesis of new molecules. The immiscibility of most polymers, because of their high molecular weight and the low entropy of large molecules, leads to heterogeneous blends and gives rise to multiphasic structures with various morphologies. The evolution of these morphologies depends on the rheological properties of each component, the volume fractions, and the interfacial tension between phases. On the basis of a simple processing technology in the melt, such as extrusion or internal batch mixing, polymer blending offers a wide range of new materials with interesting properties in biomedical,[1,2] filtration process,[3,4] and battery applications.[5–7] In these various fields, the control of the morphology is critical for the performances of the final products. A fibrillar morphology enhances the tensile properties,[8,9] a lamellar morphology yields barrier properties,[10,11] and a droplet/matrix morphology improves the impact properties.[12] Cocontinuous morphology[13–15] is a special case of morphology in binary polymer blends. This structure, where both phases percolate, has significant effects on the physical and mechanical properties, such as the conductivity and permeability properties, of polymers blends.[10,16–20] To generate these cocontinuous morphologies, it is necessary to perform blending under specific conditions in a particular composition range. A wide range of techniques has been described in the literature to detect these cocontinuity windows. One of the most used methods is the selective extraction by a solvent. Most of the time, only one component of a blend presents a selective solvent (mainly because one is a polyolefin). Anyway, such systems allow the visualization of the morphology. One component clearly appears on the micrographs, and the other one is represented by the cavities. For polyolefin blends, it is quite impossible to get information on the morphology; only few studies have proposed alternative techniques. For example, Raman

© 2012 Wiley Periodicals, Inc.

Table I. Rheological Data at 180°C of the Pure Components

	0.01 s^{-1}			25 s^{-1}		
Polymer	Viscosity (Pa s)	$\eta^*_{VdF}/\eta^*_{PEO}$	G'_{VdF}/G'_{PEO}	Viscosity (Pa s)	$\eta^*_{VdF}/\eta^*_{PEO}$	G'_{VdF}/G'_{PEO}
PVdF	420,000	148	8,400	5190	4.40	6.63
PVdF–HFP (11 wt % HFP)	84,200	30	667	3250	2.75	3.79
PVdF–CTFE (4 wt % CTFE)	630,000	222	13,000	5990	5.08	7.85
PEO	2,840	—	—	1180	—	—

η^*, complex viscosity; HFP, hexafluoropropene; CTFE, chlorotrifluoroethylene.

mapping has been used.[21] This method has been used many times in different studies, which have demonstrated its efficiency.[22–25] On the basis of the existence of a couple of selective solvents, this method is able to selectively dissolve one phase of the binary blend without affecting the other one. So, it becomes possible to study the morphology of the whole composition range of the blend. Other popular methods for studying the morphology use different types of microscopy, such as optical microscopy[26] and transmission electron microscopy.[27,28] However, the most suitable technique for the three-dimensional (3D) visualization of the morphology is scanning electron microscopy (SEM). With this technique, it is possible to complete and confirm the results from selective extraction. Complementarily, rheological studies are another suitable technique for highlighting the evaluation of the cocontinuity domain. Indeed, there is a real link between the morphology and the dynamic behavior in the melt, especially as pointed out by the storage modulus (G') at low frequencies.[22,29,30]

In this study, the morphologies of three different vinylidene fluoride (VdF) based homopolymers and copolymers mixed with poly(ethylene oxide) (PEO), were investigated with a focus on the cocontinuous domain. The objective was to use some specific tools to determine the state of the morphology in each phase of these three systems with consideration of the specificities and chemical characteristics of the materials. In the first part, the morphology of each phase of the blends was investigated by selective extraction experiments and SEM. In the second part, dynamic viscoelastic properties measurements in the melts of the blends were used to investigate the relationships between the morphology and the viscoelastic properties of the blends.

EXPERIMENTAL

Materials

In this study, innovating materials were selected to meet some appropriate criteria of immiscibility and solubility. These materials were selected according to the great potential and performance in the batteries field. Three VdF-based polymers manufactured by Arkema, France were chosen: a homopolymer [Kynar 761, poly(vinylidene fluoride) (PVdF)], a poly(vinylidene fluoride-*co*-hexafluoropropene) copolymer (PVdF–HFP), and a poly(vinylidene fluoride-*co*-chlorotrifluoroethylene) copolymer (PVdF–CTFE). These polymers were melt-mixed with PEO (number-average molecular weight = 200,000 g/mol). This water-soluble polymer was a commercial-grade polymer provided by Dow Chemicals, France. 1-Methyl-2-pyrrolidone (NMP; 99.5%, extra dry, Acros Organics, France) was used to extract the VdF-based phase. NMP had a melting point of −24°C and a boiling point of 202°C. Its molecular weight was 99.1 g/mol.

Mixing

The polymers were blended in a Haake (Germany) Rheomix 600 internal batch mixer at 180°C, with a roller speed set up at 50 rpm. This speed matched an average shear rate estimated to be 25 s^{-1}. This value was measured through a proper calibration, which allowed us to convert torque measurements and rotation speeds into shear stress and shear rate data.[31] The residence time of the compound inside the hot chamber was set at 7 min to limit PEO degradation.[32] The materials provided in powder form were first dried *in vacuo* at 40°C for 12 h and then dry-mixed in an electric blender for 1 min. The composition range of each blend extended from 100 wt % PEO- to 100 wt % VdF-based polymers with steps of 10 wt %. In all experiments, about 70% of the total volume available in the chamber was filled with material to fully optimize the mixing.

A time of 7 min of mixing appeared to be too short to establish the equilibrium morphology well, but immiscible polymer blends are not thermodynamically stable. So, we compared different quenched systems after the same conditions of mixing time, shear rate, and temperature, and we observed the differences in the morphology for the different blends.

Rheological measurements

A constant stress rheometer (TA Instruments, DE, USA SR5000) set up with a 25-mm parallel-plate fixture was used to measure the dynamic rheological properties in the melt (Table I). A frequency sweep was performed under a nitrogen atmosphere in the range of 0.01 to 100 rad/s at 180°C. For all samples, a maximum stress of 1500 Pa was used and was defined by a stress sweep test to ensure that the experiments were carried out in the linear viscoelastic domain. Figure 1 shows the results of the oscillatory experiments at 180°C for the neat components. PEO was the less elastic and the less viscous component among the polymers.

Differential scanning calorimetry (DSC)

Thermal analysis was performed with a TA Instruments, DE, USA DSC Q10 under nitrogen combined with a TA Instruments refrigerated DSC cooling system. The sample was positioned in a hermetic aluminum pan. The system was first stabilized at 20°C; then, two cycles were performed with a temperature ramp from −80 to 250°C with a heating rate of 10°C/min. The system was

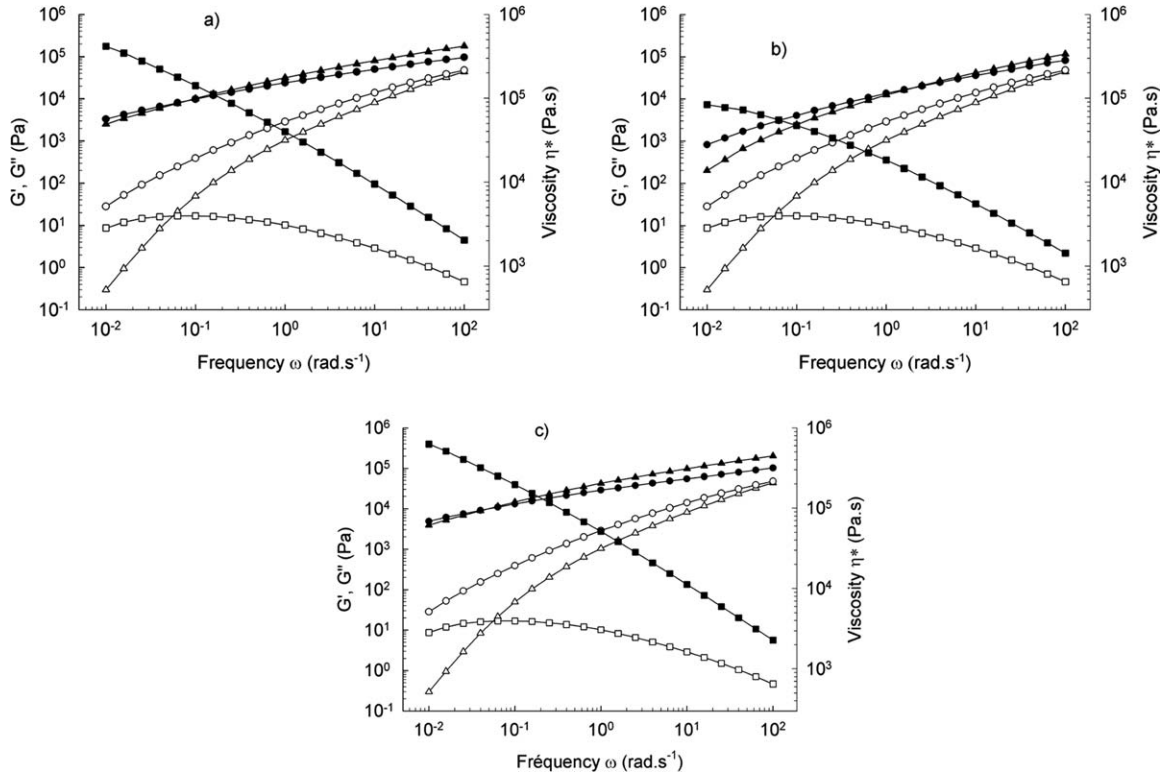

Figure 1. G' values of (▲) VdF and (△) PEO, loss moduli (G'') of (●) VdF and (○) PEO, and complex viscosity (η^*) values of (■) VdF and (□) PEO versus frequency (ω) at 180°C for (a) PVdF and PEO, (b) PVdF–HFP, and PEO, (c) PVdF–CTFE and PEO.

calibrated previously with a classical baseline measurement and constant determination with a certified indium sample.

Selective extraction experiments

The selective extraction method is a suitable technique for the study of the morphology of polymers blends. The specificity of this study was that each component was selectively removed separately with two different specific solvents. A piece of approximately 3 g of a properly shaped compact sample was weighed and then immersed in a large excess of selective solvent over 5 days under agitation. The two selective solvents were chosen carefully to dissolve completely each phase without any influence on the other one. To remove the VdF-based phase, NMP was used, whereas the PEO phase was easily removed by water. After water extraction of the PEO phase, the remaining part was taken out of the solvent and dried *in vacuo* at 35°C. For the extraction of the VdF-based polymers, the remaining part was first washed thoroughly with acetone to remove all of the solvent before drying *in vacuo* at 35°C. When the weight was found to be constant, the comparison between the original weight before extraction and the final weight after extraction was used to calculate the percentage of continuity of the component. The continuity of one phase can be described as the fraction of polymer that belongs to a continuous phase. It can be determined by the following relation:

$$\text{Continuity} = \frac{w_{\text{initial}} - w_{\text{final}}}{w_{\text{initial}} w_a} \quad (1)$$

where w_{initial} is the initial weight of the sample, w_{final} is the final weight of the sample after extraction, and w_a is the weight fraction of component *a*. If the sample is not self-supported after extraction, the amount of continuity is set to 100% and the morphology of the component is considered to be fully continuous.

SEM

SEM is an investigative and complementary technique for selective extraction experiments. To characterize the morphology of the blend, the sample was fractured in liquid nitrogen after the extraction of one phase. The fractured surfaces were coated with a gold–palladium alloy and examined by a Hitachi S3000-N scanning electron microscope at an accelerating voltage of 5 kV at low temperature (−18°C) to protect the structure of the effect of the electron beam.

RESULTS AND DISCUSSION

Thermal properties of the polymers in the blends, immiscibility, and composition

Figure 2 shows the second run of thermograms of the PVdF–HFP/PEO blends in the range 10–190°C. This range included the melting points of the two components. Two distinct melting points clearly appeared for each blend with constant temperatures whatever the composition; this demonstrated that both polymers were immiscible. Also, the area below the melting peaks of PEO grew as the volume fraction increased. On the other side, the area below the melting peaks of PVdF–HFP decreased as the volume fraction increased. The melting point of the polymers were 59°C for PEO, 166°C for PVdF, 150°C for PVdF–HFP, and 154°C for PVdF–CTFE. The enthalpies of

Table II. Calorimetric Data of the Polymers in the Different Blends

VdF (%)	Melting point (peak; °C) of the VdF-based polymers			Enthalpy of fusion (J/g) of the VdF-based polymers			Calculated composition (%) of the VdF-based polymers		
	PVdF/PEO	PVdF–HFP/PEO	PVdF–CTFE/PEO	PVdF/PEO	PVdF–HFP/PEO	PVdF–CTFE/PEO	PVdF/PEO	PVdF–HFP/PEO	PVdF–CTFE/PEO
100	166.2 ± 0.1	149.8 ± 0.1	154.3 ± 0.1	32.2 ± 0.5	15.0 ± 0.6	25.9 ± 0.5	100	100	100
70	164.3 ± 0.1	149.5 ± 0.1	154.8 ± 0.1	23.0 ± 0.2	11.0 ± 0.3	18.4 ± 0.3	71 ± 2	73 ± 1	71 ± 2
50	163.6 ± 0.1	149.6 ± 0.1	151.1 ± 0.1	14.9 ± 0.1	8.4 ± 0.3	13.4 ± 0.3	46 ± 2	56 ± 4	52 ± 1
30	165.5 ± 0.1	148.6 ± 0.6	152.1 ± 0.1	10.1 ± 0.2	4.2 ± 0.4	8.6 ± 0.3	31 ± 1	28 ± 2	33 ± 1
0	—	—	—	—	—	—	0	0	0

PEO (%)	Melting point (peak; °C) of PEO			Enthalpy of fusion (J/g) of PEO			Calculated composition (%) of PEO		
	PEO/PVdF	POE/PVdF–HFP	PEO/PVdF–CTFE	PEO/PVdF	PEO/PVdF–HFP	PEO/PVdF–CTFE	PEO/PVdF	PEO/PVdF–HFP	PEO/PVdF–CTFE
0	—	—	—	—	—	—	0	0	0
30	57.12 ± 0.1	59.6 ± 0.1	61.1 ± 0.2	32.9 ± 0.6	29.8 ± 0.5	36.1 ± 0.7	27 ± 1	25 ± 1	30 ± 1
50	57.9 ± 0.1	57.7 ± 0.1	57.8 ± 0.1	58.0 ± 4.0	51.7 ± 0.1	58.0 ± 2.0	48 ± 3	43 ± 1	48 ± 2
70	59.1 ± 0.1	59.9 ± 0.1	60.9 ± 0.1	83.9 ± 0.5	76.6 ± 0.6	86.2 ± 0.9	70 ± 1	64 ± 1	72 ± 1
100	59.0 ± 0.1	59.0 ± 0.1	59.0 ± 0.1	119.8 ± 0.7	119.8 ± 0.7	119.8 ± 0.7	100	100	100

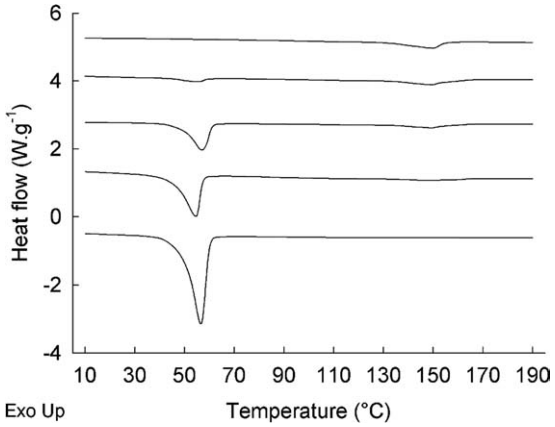

Figure 2. Thermograms of the PVdF–HFP/PEO blends (from top to bottom: 0, 30, 50, 70, and 100% PEO).

melting are also given in Table II. With the measured enthalpy for the neat polymers and for each blend, the composition could be checked. The calculated compositions are summarized in Table II. The good correspondence between the theoretical and measured percentages led us to conclude that the degree of crystallinity did not change, despite the evolution of the morphology. The small variations in the results were related only to measurement uncertainties. Some crystallinity changes were observed in dispersed droplet morphology systems by other authors, but in this study, no change was measured.

Diagrams of continuity versus composition

Selective extraction was used to establish the cocontinuity domains of the systems. Indeed, this domain could be determined by the use of a diagram of continuity, which presents the percentage of continuity of each phase, calculated from eq. (1), as a function of the blend composition for the three systems [Figure 3(a–c)]. The domain highlighted in this figure could be described as the composition range in which each phase was continuous and where both phases coexisted in the same volume. The selected criteria to draw the borders of the zone were 80% continuity. The sample shows two cocontinuous and distinct structures.[15]

The three diagrams present the same sigmoidal shape pointed out by the solid black line. Three different zones could be distinguished for each curve. For each polymer, at low contents, the percentage of continuity was near to zero. The system could considered to have a droplet/matrix morphology. As the content of the selected component increased, the curve rose up quickly. A percolation threshold appeared that corresponded to the creation of the first connections between droplets, where a 3D structure began to appear. At high contents of the component, its continuity was nearly 100%. The 3D structure was fully established, and the morphology of the polymer was fully continuous. However, before that, the morphology was only partially continuous. In this case, some droplets still coexisted with the percolated structure. It has to be noted here that the same continuity diagrams do not mean the same characteristic size of the morphology. Both systems could have the same

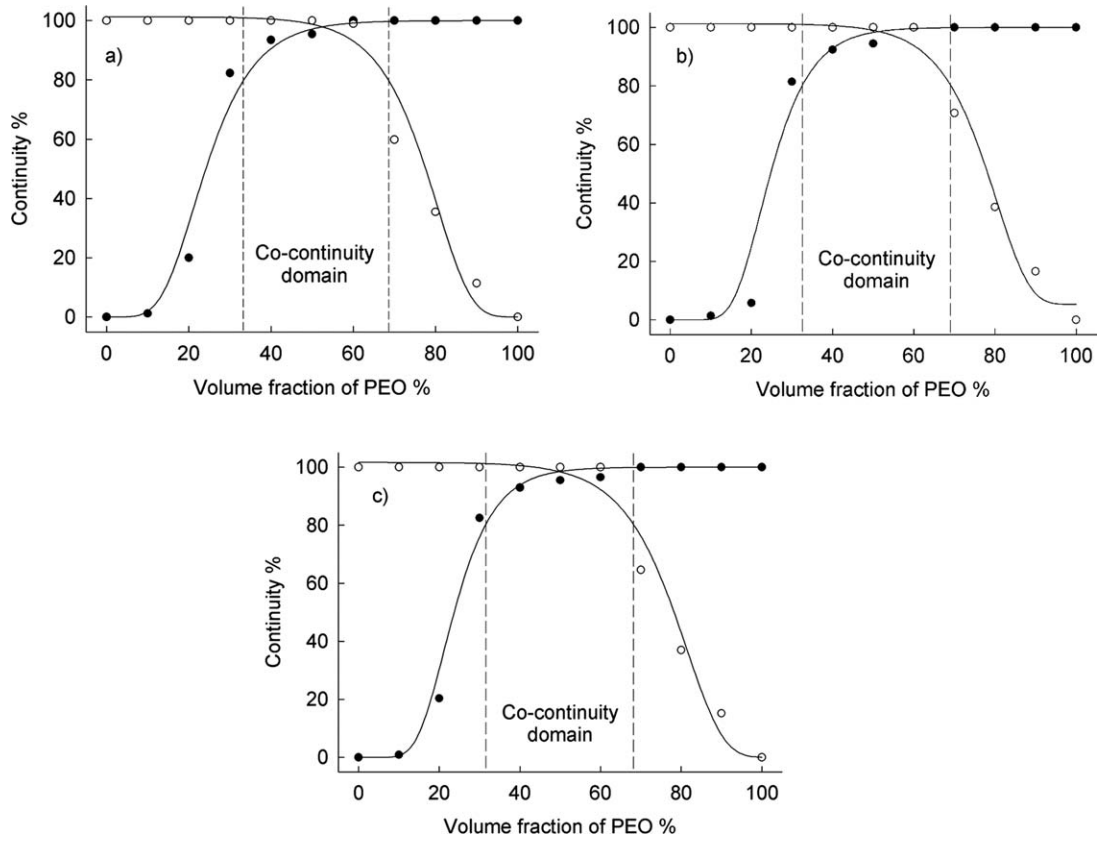

Figure 3. Diagrams of continuity for (a) PVdF/PEO, (b) PVdF–HFP/PEO, and (c) PVdF–CTFE/PEO: (●) PEO extraction and (○) VdF-based polymer extraction.

cocontinuous composition but two different sizes of interconnected phases.

The extraction curves appeared very similar for the PVdF/PEO, PVdF–HFP/PEO, and PVdF–CTFE/PEO systems and overlapped almost perfectly (Figure 4). Despite the differences in rheological data, different viscosities, and different viscosity ratios, these systems gave identical morphologies. The onset of percolation (when the continuity curve strongly increased from zero) of PEO occurred just above 15% for each system. On the other side, the VdF-based polymers seemed to percolate at around 10%. According to different definitions listed in other studies,[15,33,34] the continuity domain generally extends from 30 to 65% of PEO. As pointed out by Lyngaae–Jorgensen, Utraki, and coworkers,[33,34] this specific range was consistent with the percolation theory. Actually, the structures formed by melt mixing involved a set of different types of morphologies rather than an ideal and unique continuous structure. The continuity domain can also be defined as the composition range that is bounded on each side by a structure in which at least a part of each phase forms a continuous structure that percolates the whole volume.

Morphologies in connection with the diagrams of continuity

To complete the selective extraction experiments, samples were observed by SEM after extraction. The morphologies of the various blends were confirmed. Figure 5 shows the SEM images of

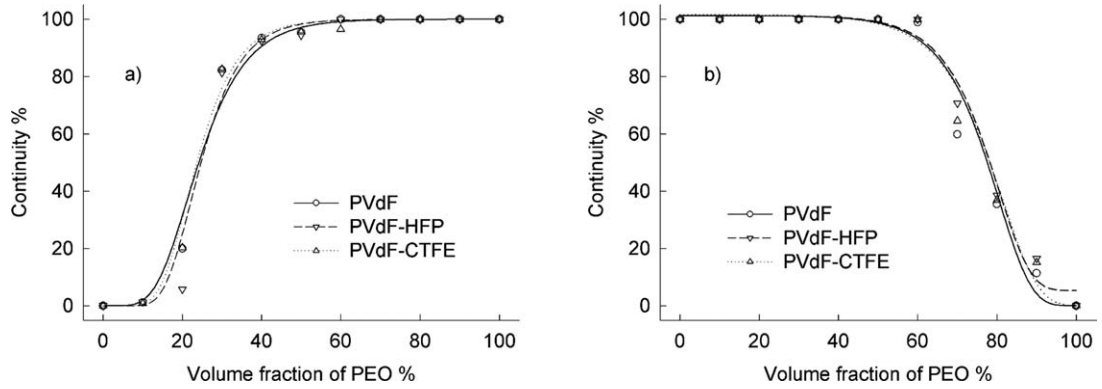

Figure 4. Overlay of the extraction curves for the three systems: (a) PEO extraction and (b) VdF-based polymer extraction.

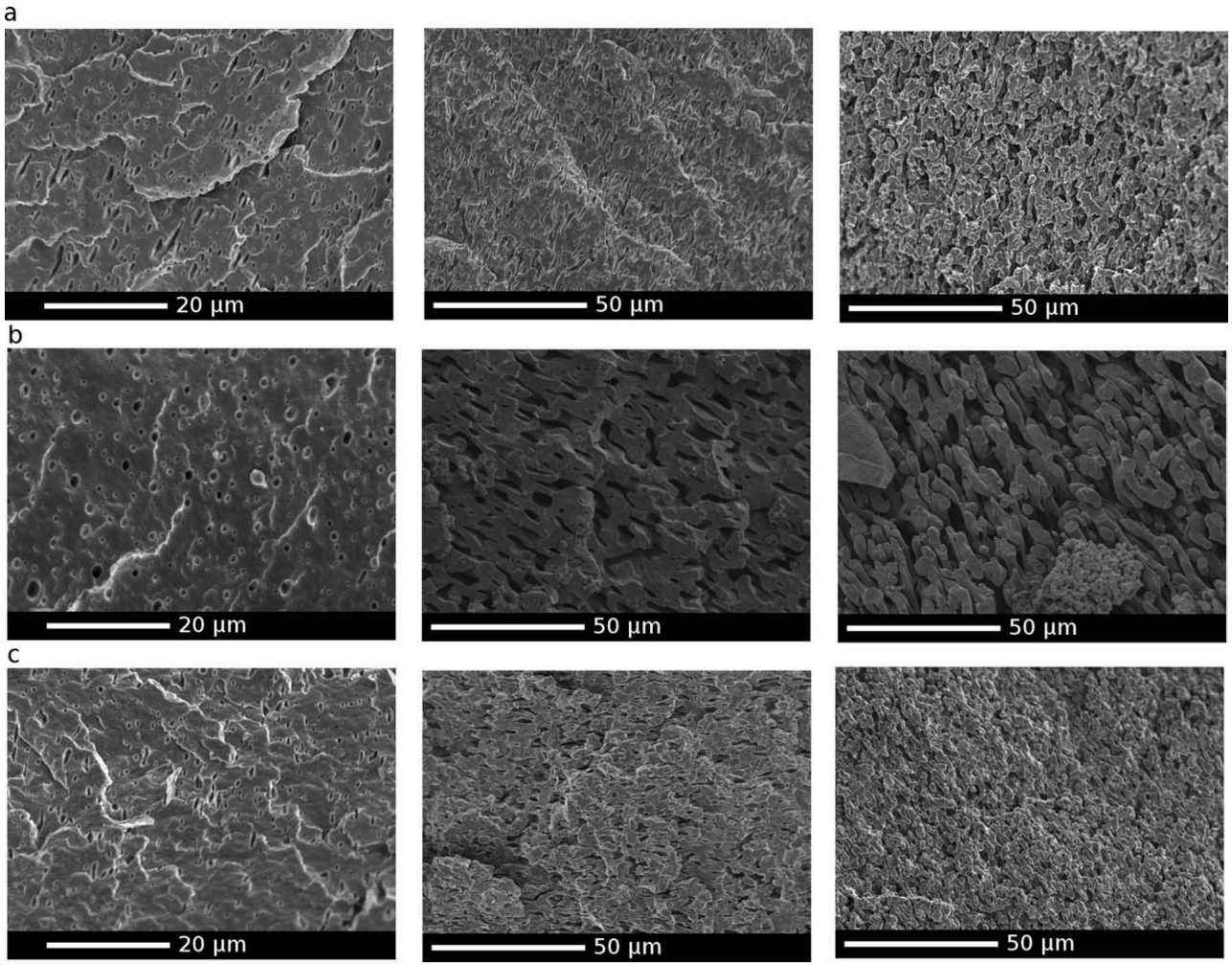

Figure 5. SEM images of the (a) PVdF, (b) PVdF–HFP, and (c) PVdF–CTFE phases after the extraction of PEO. The content of PEO increases from left to right (10, 30, and 50%).

VdF-based polymer blends with 10, 30, and 50 wt % PEO after the extraction of the PEO phase. Only the remaining VdF-based polymers were visible. As expected, the morphology of the dispersed PEO droplets in the matrix was clearly observed for the three systems with 10% PEO [Figure 5(a–c), left]. The prints of nodules remaining after extraction were visible as small holes in these images. Figure 5(a–c) (middle) shows the morphology at the beginning of the continuity domain, where the PEO phase started to form thin threads of a cocontinuous structure at 30% PEO. The morphology was partially cocontinuous. At 50% PEO [Figure 5(a–c), right], the morphology was fully cocontinuous.

The advantage of the double-selective extraction relies on the possibility of obtaining SEM images of each phase alternatively. Thereby, in Figure 6, the images represent the PEO matrix after the extraction of the VdF-based polymer phases and show the second part of the diagram of continuity. Figure 6(a–c) (right) shows the morphology of the dispersed VdF-based polymer droplets in the PEO matrix at 90% PEO. With the decrease in the content of PEO, the holes grew and expanded until they finally percolated at the second boundary of the continuity domain at 60% PEO [Figure 6(a–c), middle]. Figure 6(a–c) (left) shows the fully cocontinuous zone, where both phases were cocontinuous at 40% PEO. The observations of the three systems gave the same results, and the curves of continuity were similar.

Although the evolution of the morphology was the same for all three systems, the three sets of images showed differences in the size of the 3D structure. This size could be compared by calculating the surface area of the hole left by the extracted phase. In the droplet/matrix zone, the surface area of the droplets was between 0.1 and 3 μm^2 for all systems. In contrast, in the continuity domain, the characteristic size was different. Indeed, the surface area of the structure was between 0.5 and 2.0 μm^2 for PVdF and PVdF–CTFE, but it was much larger (10 and 25 μm^2) for PVdF–HFP. This difference in the size was clearly visible in the SEM images. It could be explained by the lower viscosity of PvdF–HFP (Table I).

The viscosity of the matrix is directly related to the size of the droplets via the capillary number, Ca. With eq. (2), one can say that when Ca is weak, the interfacial strengths are bigger than the deformation stress, then a stable droplet will develop. So when the matrix viscosity is low, it becomes impossible to break the droplets into smaller ones, and the morphology appears bigger:

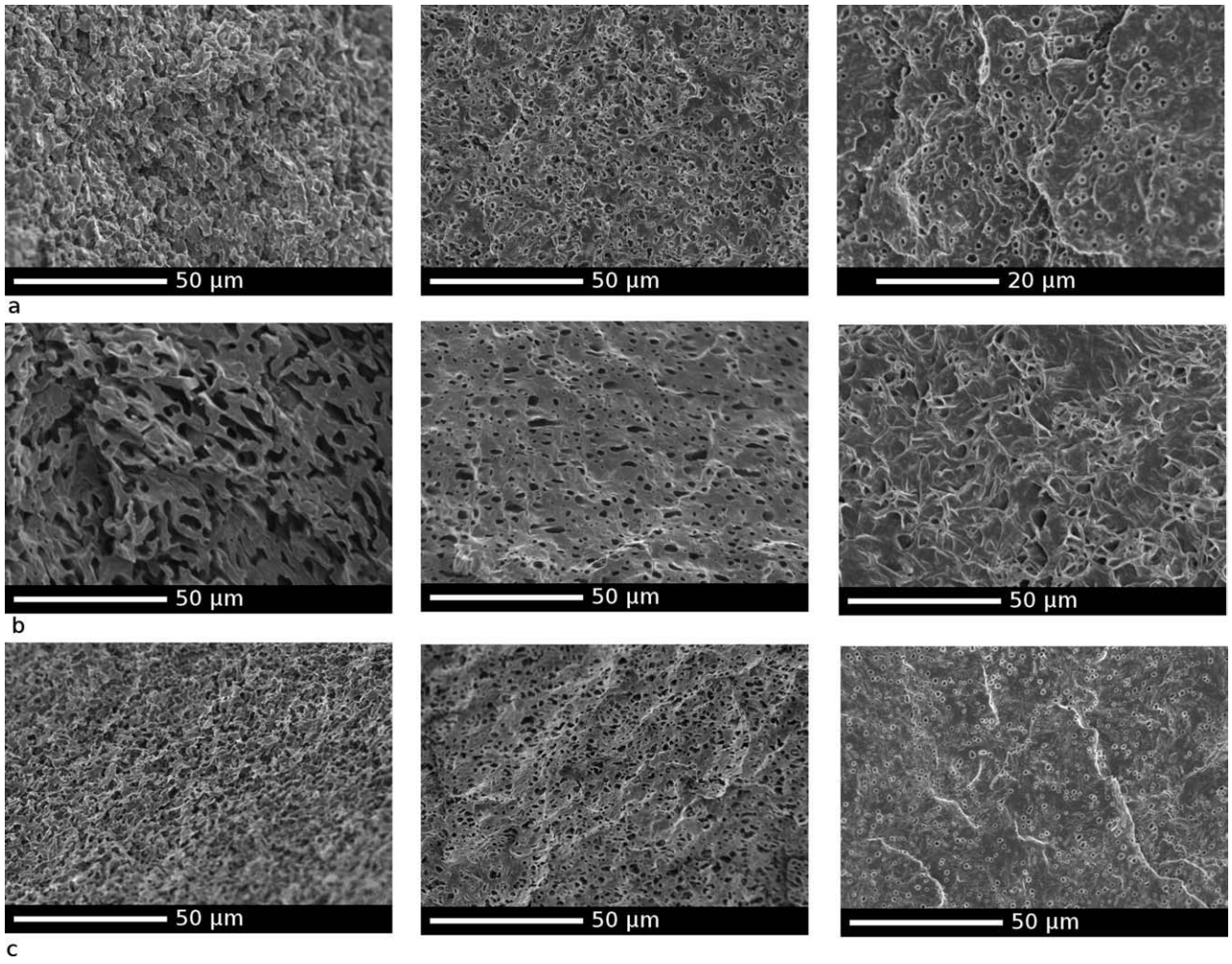

Figure 6. SEM images of the PEO phase after the extraction of (a) PVdF, (b) PVdF–HFP, and (c) PVdF–CTFE. The content of PEO increases from left to right (40, 60, and 90%).

$$C_a = \frac{\eta_m R\dot{\gamma}}{\sigma} \quad (2)$$

where R is the droplet radius, σ is the interfacial tension, η_m is the viscosity of the matrix, and $\dot{\gamma}$ is the shear rate.

The same explanation works for more complicated morphologies, such as cocontinuous ones.

Table I shows the determining rheological data for the morphology setup of the blends within the blending conditions.

Low-frequency elasticity in the melt associated with interface and low-frequency relaxations

The dynamic behavior in the molten state of the blends was measured over the whole composition range. The plots of G' as a function of the composition and frequency (Figure 7) revealed a pseudo-plateau that was visible at low frequencies. This elasticity could not be connected to the elasticity of the neat polymers only because it was far larger than what was predicted by the simple blending law. As shown in many studies,[22,30] this elasticity in excess can only be explained by the existence of complex morphologies in blends, and it is related to the presence of an interface. Because of the interfacial tension between the components, the energy is stored within the deformed phase. Then, when this out-of-equilibrium deformed structure is solicited, extra elasticity appears. As soon as this excess of interfacial area exists in the strained deformable two-phase blend, the elasticity is increased. This was observed for the blends under investigation over the whole composition range, except for the neat polymers.

However, usually, the relaxation of shape and the return to equilibrium should be observed as described by Palierne[35] in the case of droplet/matrix morphologies. In this work, the low-frequency elasticity relaxation is not observed, and the frequency–modulus curves show a plateau rather than a shoulder associated with a particular relaxation time. It does not mean that Palierne's model fails to describe our system; it simply shows that the frequency window used for the characterization at this temperature was not adequate. The relaxation of the droplets should require either a higher temperature or a lower frequency to be observed, but such experimental conditions were not compatible with regard to PEO degradation issues.

The theoretical expected shape relaxation time (τ_D) was calculated with the effect of droplet size, the interfacial tension between the components, and the viscosity and viscosity ratio according to eq. (3) for Newtonian fluids taken into account:[35]

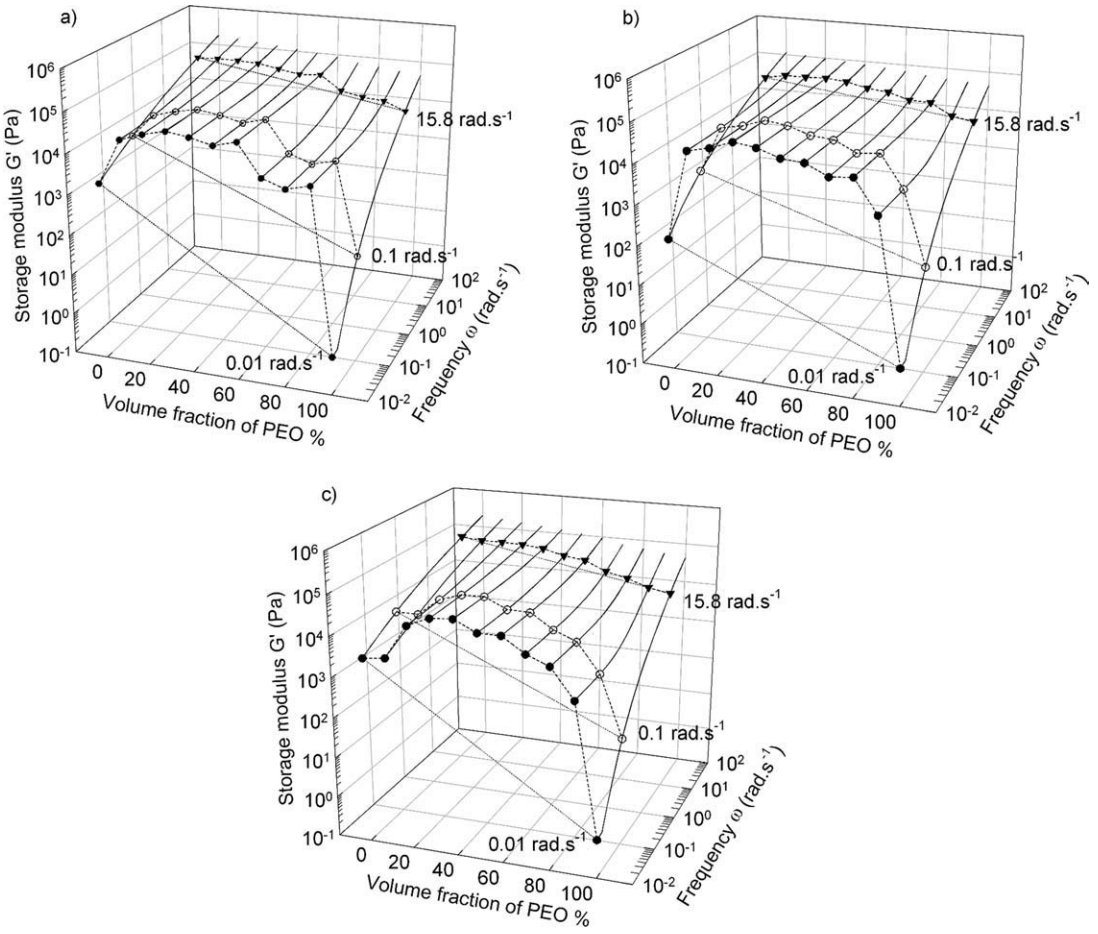

Figure 7. (●) G' at 0.01, (○) 0.1, and (▼) 15.8 rad/s for (a) PVdF/PEO, (b) PVdF–HFP/PEO, and (c) PVdF–CTFE/PEO at 180°C for the complete composition range.

$$\tau_D = \frac{\eta_{0m} R}{4\gamma_{12}} \frac{[(19p_0 + 16)(2p_0 + 3 - 2\Phi(p_0 - 1)]}{[10(p_0 + 1) - 2\Phi(5p_0 + 2)]} \quad (3)$$

where η_{0m} is the zero-shear viscosity of the matrix, R is the size of the dispersed phase, Φ is the volume fraction of dispersed phase, γ_{12} is the interfacial tension, and p_0 is the viscosity ratio at zero-shear rate.

For the various systems, the interfacial tensions were calculated with eq. (4) of Owens and Wendt[36] and Kaelble.[37] For the polymers under investigation, only the values of γ the surface tension, γ^d the dispersive interactions, and γ^p the polar interactions for PEO, PVdF, PVdF–HFP, and PVdF–CTFE were known from the literature.[38–41] A simple mixing law [eq. (5)] was used to calculate these values for the copolymers:

$$\gamma_{12} = \gamma_1 + \gamma_2 - 2\sqrt{\gamma_1^d \gamma_2^d} - 2\sqrt{\gamma_1^p \gamma_2^p} \quad (4)$$

$$\gamma_{copo} = \gamma_{poly1} \times w\%_{poly1} + \gamma_{poly2} \times w\%_{poly2} \quad (5)$$

Where are respectively the surface tension, the dispersive interaction and the polar interaction of polymer 1 and polymer 2. Where are respectively the surface tension of the copolymer and the surface tensions of polymer 1 and polymer 2. $w\%_{poly1}$ and $w\%_{poly2}$ are the weight fractions of polymer 1 and 2.

Table III gives the results of the calculation of interfacial tension. Table IV indicates the values of τ_D at 10 vol % droplets on both sides of the composition range with the values of Table IV. The low-frequency data of the viscosity were taken as an approximation of the zero-shear rate viscosity. The volume-average particle dimensions were measured with the SEM pictures and were found to be nearly 1.5 μm for all of the systems. The relaxation times of the neat polymers are also indicated.

This calculation showed that, in this study, the low-frequency elasticity relaxation could not be observed under these conditions. Indeed, because of the high viscosity of the VdF-based polymers, the relaxation time of the droplets or of the interface was high (>100 s). However, the lowest frequency used for the dynamic rheology measurements was 0.01 rad/s; this allowed only the characterization of phenomenon having relaxation times shorter than 100 s. This was connected to the peculiarity of the systems highlighted by the plot of the elasticity toward the blend composition in Figure 8. G' at 0.01 rad/s showed little variation with the composition as soon as both phases coexisted. This has also seldom been reported in the literature, where one or two maximum have generally been observed, for example, by Galloway and Macosko,[42] Huitric et al.,[29] or Castro and coworkers.[22,30] These differences were connected to the limited frequency ranges that were investigated

Table III. Interfacial Tensions of the Investigated Polymers

Polymer	PEO	PVdF	Polyhexafluoropropene	PCTFE	PVdF–HFP 11 wt %	PVdF–CTFE 4 wt %
γ (mJ/m^2)	42.8	33.8	17.0	30.9	32.0	33.7
γ^d (mJ/m^2)	30.6	31.1	14.0	22.2	29.2	30.7
γ^p (mJ/m^2)	12.2	2.7	3.0	8.7	2.7	2.9
$\gamma_{VdF/POE}$ (mJ/m^2)	—	3.4	6.3	1.0	3.5	3.3

Table IV. Interfacial Relaxation Times of the Systems at 10% Dispersed Phase

Matrix	Droplet	τ_D (s)	Matrix relaxation time (s)	Dispersed polymer relaxation time (s)
PEO	PVdF	89	1	>100
PEO	PVdF–HFP	18	1	25
PEO	PVdF–CTFE	137	1	>100
PVdF	PEO	124	>100	1
PVdF–HFP	PEO	25	25	1
PVdF–CTFE	PEO	192	>100	1

because, in this case, the shape relaxation of the phases was out of the experimental window.

When the curves obtained by selective extraction were superimposed over the low-frequency elasticity, it did not show a particular connection to the cocontinuity domain. Consequently, the elasticity was not a reliable trace of the blend morphology for such systems with a large zero-shear viscosity, large p_0, and very long τ_D.

Comonomers and cocontinuity window

From the results of selective extraction, SEM, and the viscoelastic behavior in the melt, it was definitely clear that the variation in the chemical structure and of the comonomers did not influence the boundaries of the continuity domains or the elastic behavior at low frequency for the systems examined in this study. This was consistent with the model proposed by Castro et al.[22] in 2004 and derived from a classical balance between rupture and coalescence with the approach proposed by Tokita.[43] From this model, eq. (6) for the boundary of the continuity window (Φ^*) was proposed:

$$\Phi^* = \frac{\eta_m \pi \dot{\gamma}}{4PE} / (1 + \frac{3\eta_m \dot{\gamma}}{Ca_c E}) \quad (6)$$

where η_m is the viscosity of the major phase in the mixing conditions (shear rate and temperature), P is the probability of coalescence, E is the cohesive rupture energy of the melt (minor phase), and Ca_c is the critical capillary number, which depends on the viscosity ratio in the mixing conditions.

In the absence of compatibilizer, P can be taken as 1 because any collision event may lead to coalescence. Ca_c in shear flow was calculated according to De Bruijn.[44] First, this equation does not depend explicitly on the interfacial tension between the components of the blends. Therefore, this is one of the reasons for the independence of the boundaries of the continuity domain toward the composition of the VdF-based polymers. Anyway, for the systems in this study, the calculation and results of Table I did not show large differences between the fluoropolymers from this point of view. Second, when PEO was the major phase, the viscosity ratio was very large so that Ca_c in shear was infinite for PVdF and PVdF–CTFE and large for PVdF–HFP. Therefore, on the right side of the continuity diagram, the boundary limit was defined by

$$\Phi^* = \frac{\eta_{PEO} \pi \dot{\gamma}}{4E_{VdF}} \quad (7)$$

For a similar rupture energy, which was consistent with a similar surface tension in the polymers, the boundary did not depend on the dispersed VdF-based component of the blend. From the experimental value of this boundary, the energy for rupture of melts of the VdF-based polymers (E_{VdF}) was estimated to be between 60 and 80 kJ/m^3. When PEO was the minor phase, Ca_c was nearly unity for all blends. Equation (6) can be rewritten as follows:

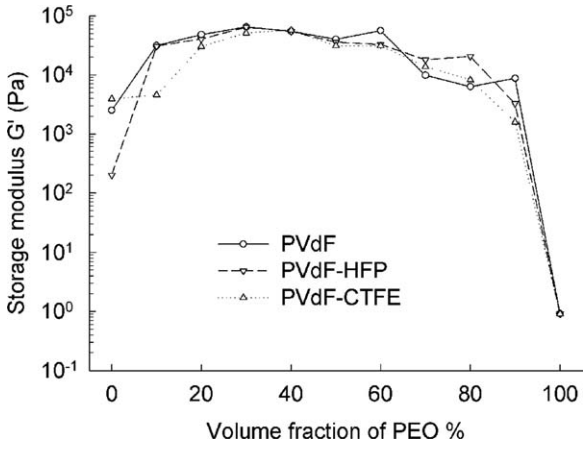

Figure 8. Comparison between G' at 0.01 rad/s for PVdF, PVdF–HFP, and PVdF–CTFE for the complete composition range.

$$\Phi^* = \frac{\eta_{VdF}\pi\dot{\gamma}}{4E_{PEO}}/(1+\frac{3\eta_{VdF}\dot{\gamma}}{E_{PEO}}) \quad (8)$$

With the energy of rupture of 300 kJ/m^3 already proposed by Castro,[22] the boundary of the domain was in the experimental range, although the predicted boundary was not really constant from one system to another.

CONCLUSIONS

In this study, the morphology and cocontinuity domain of VdF-based polymer/PEO blends were investigated. With the use of appropriate selective solvents, the morphology was characterized for each composition of the system and was confirmed by SEM. Whatever the type of VdF-based polymer or copolymer, all systems showed the same continuity curves, that is, the percentage of continuity of one component versus the blend composition. The cocontinuity zone, as defined in Potschke and Paul,[15] was between 30 and 70% PEO.

Viscoelastic measurements in oscillatory shear did not prove to be a useful tool in this case for determining the composition domain of continuity. This was in contradiction with previous work in the literature. Although the elasticity in the low-frequency domain was expected to depend on the morphology, the high viscosity of the VdF-based polymers in this study and the high viscosity ratio prevented the shape relaxation of the phases. Therefore, a pseudo-plateau was observed on G' at low frequency whatever the composition, and the excess of elasticity due to interfacial area was hidden by the elasticity of the blend components. The similarity in behavior for all of the VdF-based polymers was also reflected by the rheological study.

Finally, the similarities between the blends, whatever the VdF-based polymer, as assessed by rheological techniques, selective dissolution, and SEM observations, showed that that the chemical nature of the polymers was of minor importance in comparison to the rheological characteristics in these studied blends.

REFERENCES

1. Washburn, N. R.; Simon, C. G.; Tona, A.; Elgendy, M. H.; Karim, A.; Amis, E. J. *J. Biomed. Mater. Res.* **2002,** *60*, 20.
2. Bramfeldt, H.; Sarazin, P.; Vermette, P. *J. Biomed. Mater. Res. A* **2009,** *91*, 305.
3. Riscanu, D.; Favis, B. D.; Feng, C.; Matsuura, T. *Polymer* **2004,** *45*, 5597.
4. Matsuura, T. Synthetic Membranes and Membrane Separation Processes; CRC: Boca Raton, FL, **1993.**
5. Winter, M.; Brodd, R. *J. Chem. Rev.* **2004,** *104*, 4245.
6. Bernd, W. Investire-Network Home Page. http://www.itpower.co.uk/investire/ (accessed November 22, **2011).**
7. Arora, P.; Zhang, Z. *Chem. Rev.* **2004,** *104*, 4419.
8. Padilla-Lopez, H.; Vázquez, M. O.; González-Núñez, R.; Rodrigue, D. *Polym. Eng. Sci.* **2003,** *43*, 1646.
9. Shields, R. J.; Bhattacharyya, D.; Fakirov, S. *J. Mater. Sci.* **2008,** *43*, 6758.
10. Faisant, J. B.; Aït-Kadi, A.; Bousmina, M.; Deschênes, L. *Polymer* **1998,** *39*, 533.
11. Lape, N. K.; Mao, H.; Campera, D.; Hillmyer, M. A.; Cussler, E. L. *J. Membr. Sci.* **2005,** *259*, 1.
12. Yeniova, C. E.; Yilmazer, U. *Polym. Compos.* **2010,** *31*, 1853.
13. Willemse, R. C.; Posthuma de Boer, A.; Van Dam, J.; Gotsis, A. D. *Polymer* **1999,** *40*, 2175.
14. Li, J.; Favis, B. D. *Polymer* **2001,** *42*, 5047.
15. Pötschke, P.; Paul, D. R. *J. Macromol. Sci. Polym. Rev.* **2003,** *43*, 87.
16. Evstatiev, M.; Fakirov, S.; Schultz, J. M.; Friedrich, K. *Polym. Eng. Sci.* **2001,** *42*, 192.
17. Friedrich, K.; Ueda, E.; Kamo, H.; Evstatiev, M.; Krasteva, B.; Fakirov, S. *J. Mater. Sci.* **2002,** *37*, 4299.
18. Mamunya, Y. P. *J. Macromol. Sci. Phys.* **1999,** *38*, 615.
19. Pillin, I.; Feller, J. F. *Macromol. Mater. Eng.* **2006,** *291*, 1375.
20. Droval, G.; Feller, J. F.; Salagnac, P.; Glouannec, P. *Smart Mater. Struct.* **2008,** *17*, 1.
21. Furukawa, T.; Sato, H.; Kita, Y.; Matsukawa, K.; Yamaguchi, H.; Ochiai, S.; Siesler, H.; Ozaki, Y. *Polymer* **2006,** *38*, 1127.
22. Castro, M.; Carrot, C.; Prochazka, F. *Polymer* **2004,** *45*, 4095.
23. Bourry, D.; Favis, B. D. *J. Polym. Sci. Part B: Polym. Phys.* **1998,** *36*, 1889.
24. Bu, W.; He, J. *J. Appl. Polym. Sci.* **1996,** *62*, 1445.
25. He, J.; Bu, W.; Zeng, J. *Polymer* **1997,** *38*, 6347.
26. Weis, C. *Polym. Bull.* **1998,** *40*, 235.
27. Heeschen, W. A. *Polymer* **1995,** *36*, 1835.
28. Vinckier, I.; Laun, H. M. *Rheol. Acta.* **1999,** *38*, 274.
29. Huitric, J.; Médéric, P.; Moan, M.; Jarrin, J. *Polymer* **1998,** *39*, 4849.
30. Castro, M.; Prochazka, F.; Carrot, C. *J. Rheol.* **2005,** *49*, 149.
31. Brouillet-Fourmann, S.; Carrot, C.; Mignard, N.; Prochazka, F. *Appl. Rheol.* **2002,** *12*, 192.
32. Malik, P.; Castro, M.; Carrot, C. *Polym. Degrad. Stab.* **2006,** *91*, 634.
33. Lyngaae-Jorgensen, J.; Rasmussen, K. L.; Chtcherbakova, E. A.; Utracki, L. A. *Polym. Eng. Sci.* **1999,** *39*, 1060.
34. Utracki, L. A. *J. Rheol.* **1991,** *35*, 1615.
35. Palierne, J. F. *Rheol. Acta.* **1990,** *29*, 204.
36. Owens, D.; Wendt, R. *J. Appl. Polym. Sci.* **1969,** *13*, 1741.
37. Kaelble, D. *J. Adhes.* **1970,** *2*, 66.
38. Roe, R. J. *J. Phys. Chem.* **1968,** *72*, 2013.
39. Boulange-Petermann, L. Contact Angle; Wettability and Adhesion; K. L. Mittal, Ed.; VSP: Utrecht; The Netherlands, **2003; Vol.** *3*, p 509.
40. Wu, S. *J. Polym. Sci. Part C: Polym. Symp.* **1971,** *34*, 19.
41. Schonhorn, H.; Ryan, F. W.; Sharpe, L. H. *J. Polym. Sci. Part A-2: Polym. Phys.* **1966,** *4*, 538.
42. Galloway, J. A.; Macosko, C. W. *Polym. Eng. Sci.* **2004,** *44*, 714.
43. Tokita, N. *Rubber Chem. Technol.* **1977,** *50*, 292.
44. De Bruijn, R. A. Ph. D. Thesis, University of Technology, Eindhoven, **1989.**